

Article

Intelligent Inversion Analysis of Surrounding Rock Parameters and Deformation Characteristics of a Water Diversion Surge Shaft

Xing-Wei Zou¹, Tao Zhou², Gan Li^{3,*}, Yu Hu⁴, Bo Deng² and Tao Yang²¹ Sino-Hydro Bureau 5 Co., Ltd., Chengdu 610200, China; zouxingwei@126.com² Sichuan Qingyuan Engineering Consultants, Chengdu 610015, China; zhoutao@qyec.com.cn (T.Z.); dengbo@qyec.com.cn (B.D.); yanghongkun@qyec.com.cn (T.Y.)³ School of Civil & Environmental Engineering and Geography Science, Ningbo University, Ningbo 315000, China⁴ State Key Laboratory of Hydrosience and Engineering, Tsinghua University, Beijing 100084, China; huyu93@tsinghua.org.cn

* Correspondence: ligan303@126.com; Tel.: +86-159-1095-7882

Abstract: The water diversion surge shaft is vital for a hydropower station. However, the complex geological properties of the surrounding rock make it challenging to obtain its mechanical parameters. A method combining particle swarm optimization (PSO) and support vector machine (SVM) algorithms is proposed for estimating these parameters. According to the engineering geological background and support scheme, a three-dimensional model of the water diversion surge shaft is established by FLAC3D. An orthogonal test is designed to verify the accuracy of the numerical model. Then, the surrounding rock mechanical parameter database is established. The PSO-SVM intelligent inversion algorithm is used to invert the optimal values of the mechanical parameters of the surrounding rock. The support for excavating the next layer depends on the mechanical parameters of the current rock layer. An optimized design scheme is then compared and analyzed with the original support scheme by considering deformation and plastic characteristics. The research results demonstrate that the PSO-SVM intelligent inversion algorithm can effectively improve the accuracy and efficiency of the inversion of rock mechanical parameters. Under the influence of excavation, the surrounding rock in the plastic zone mainly fails in shear, with maximum deformation occurring in the middle and lower parts of the excavation area. The maximum deformation of the surrounding rock under support with long anchor cables is 0.6 cm less than that of support without long anchor cables and 4.07 cm less than that of support without an anchor. In the direction of the maximum and minimum principal stress, the maximum depth of the plastic zone under the support with long anchor cables is 1.3 m to 2.6 m less than that of the support without long anchor cables and the support without an anchor. Compared with the support without long anchor cables and support without an anchor, the support with long anchor cables can effectively control the deformation of the surrounding rock and limit the development of the plastic zone.

Keywords: water diversion surge shaft; parameter inversion; numerical simulation; particle swarm optimization; support vector machine



Citation: Zou, X.-W.; Zhou, T.; Li, G.; Hu, Y.; Deng, B.; Yang, T. Intelligent Inversion Analysis of Surrounding Rock Parameters and Deformation Characteristics of a Water Diversion Surge Shaft. *Designs* **2024**, *8*, 116. <https://doi.org/10.3390/designs8060116>

Academic Editor: Pedro Aires Montenegro

Received: 10 October 2024

Revised: 30 October 2024

Accepted: 1 November 2024

Published: 6 November 2024



Copyright: © 2024 by the authors. Licensee MDPI, Basel, Switzerland. This article is an open access article distributed under the terms and conditions of the Creative Commons Attribution (CC BY) license (<https://creativecommons.org/licenses/by/4.0/>).

1. Introduction

As an important part of a water diversion hydropower station, the stability of the surrounding rock of the water diversion surge shaft directly affects the safety of its operation [1,2]. Affected by factors such as rock properties and ground stress, the surrounding rock safety of deep underground tunnels will face various safety threats [3–5]. Since surge shafts are usually located in complex geological conditions, the mechanical properties of the surrounding rock usually show nonlinearity, heterogeneity and anisotropy [6–8], resulting

in the acquisition of mechanical parameters of surrounding rock, and the prediction of its deformation characteristics is a major problem in engineering design. Although traditional indoor tests and in situ tests can provide some information on surrounding rock mechanical parameters, they are difficult to carry out due to the complex construction environment, large engineering volume and lack of large-scale in situ monitoring [9,10]. Especially in deep underground projects, the variability and uncertainty of surrounding rock parameters make the construction potentially dangerous [11–13]. Therefore, a method that can efficiently and accurately obtain surrounding rock parameters has important application value in practical engineering.

Traditional inversion methods make it difficult to handle complex nonlinear problems and are also inefficient. The intelligent inversion method is data-based, combining traditional numerical simulation and modern machine learning intelligent algorithms. By learning from measured data, the optimal solution can be found in the multidimensional parameter space, and the efficient identification of engineering parameters can thereby be realized. This method not only breaks through the high dependence of traditional inversion methods on initial values and objective functions but also can handle engineering problems under highly nonlinear, multidimensional and complex boundary conditions. However, it has high requirements for computer numerical simulation technology and big data processing capabilities. With the rapid development of artificial intelligence technology and computer science, numerical simulation [14–18] and machine learning algorithms [19–22] have been widely used in tunnel engineering and deep geological engineering. Parameter identification and prediction methods in the field of geotechnical engineering have entered a new stage. Based on the XGBoost model, a macro parameter prediction and micro parameter inversion model is established, which can solve the complicated macro and micro parameter calibration problem in the discrete element method simulation of rock mechanics [23]. To obtain rock creep parameters, a secondary particle swarm optimization (PSO) for rheological parameters inversion is proposed by Yang et al. [24]. According to the wavelet analysis theory, the support vector machine (SVM) method is used to perform inverse calculations on geotechnical mechanics by Ruan et al. [25], and the particle swarm algorithm is applied to optimize the parameter function. An improved adaptive particle swarm optimization with a neural network algorithm is proposed to realize the back analysis of tunnel surrounding rock mechanical parameters based on the displacement information of the engineering site [26]. Among various intelligent algorithms, particle swarm optimization and support vector machine have gradually become the mainstream methods in the inversion of surrounding rock parameters due to their excellent performance in global search and classification capabilities, and many new algorithms have been derived according to engineering needs. Chen et al. [27] use PSO to optimize velocity inversion and improve the imaging accuracy of the surface wave while using a tunneling method for predicting geological structures. A new back-analysis method of rock mechanical parameters combining the LS-SVM model and Littlewood–Paley wavelets is proposed by Wang et al. [28]. Using PSO to estimate the optimal rheological parameter set, Kovacevic et al. [29] establish a prediction model for the medium- and long-term vertical settlement performance of soft rock tunnels based on their self-developed neural network NetRHEO. VGGNet, ResNet and SVM are used by Ma et al. [30] to establish surrounding rock classification models, among which the SVM classifier had the highest accuracy, revealing that the SVM classification model has greater robustness in learning and generalizing small samples and unbalanced samples. Based on the area under the curve method, it is found that the prediction accuracy of the coupled model for landslide susceptibility assessment is significantly better than that of the single information volume model and the SVM model [31]. Zhang et al. [32] developed an intelligent optimization algorithm that combines PSO and Gaussian process (GP) theory. Then, the finite difference method (FDM) is applied to form a PSO-GP-FDM displacement inversion analysis method. Yan et al. [33] propose an improved Gaussian process regression (IGPR) with combinatorial kernel functions by adding two

mononuclear functions. Combining PSO with the IGPR model, the PSO algorithm can be employed directly to search for the optimal rock force parameters.

While many studies focus on inverting rock mechanical parameters using machine learning, there is a lack of research specifically addressing the inversion of these parameters for the stratified excavation of the water diversion surge shaft. To perform rock mechanical parameter inversion more accurately and efficiently, the particle swarm optimization and support vector machine are combined to propose a new rock mechanical parameter inversion method. Using the PSO-SVM rock mechanical parameter inversion method, a three-dimensional numerical model of the water diversion surge shaft excavation process is established by FLAC3D. By inversely analyzing the mechanical parameters of the surrounding rock of the water diversion surge shaft, its deformation and plasticity characteristics will be studied to provide a scientific basis and technical support for the design and safety assessment of deep underground engineering.

2. PSO-SVM Inversion Method of Rock Mechanical Parameters

2.1. PSO Method

Particle Swarm Optimization is a global optimization algorithm based on population intelligence [34]. The principle of PSO is shown in Figure 1. It originated from the study of the foraging behavior of bird flocks and was proposed by Kennedy and Eberhart in 1995 [35]. PSO has several advantages, including its easy implementation, few parameters and strong global search ability. It is suitable for solving complex nonlinear and multi-parameter inverse problems and has been widely used in function optimization, neural network training and combinatorial optimization [36,37].

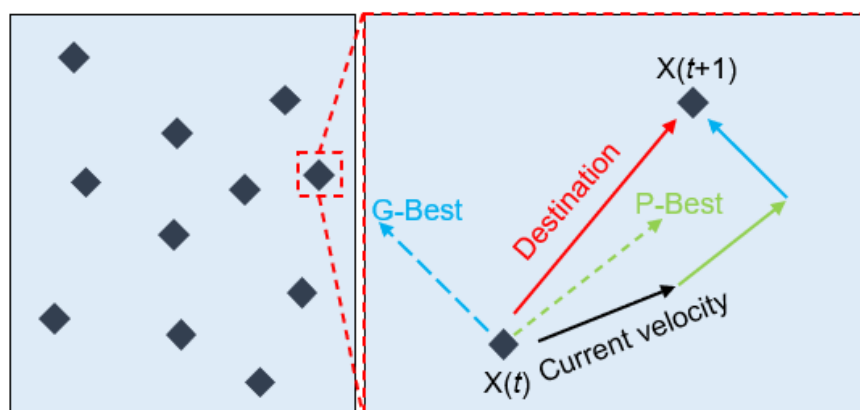


Figure 1. Schematic diagram of particle swarm optimization.

PSO realizes the search for a globally optimal solution through the following four steps.

- (1) Generating a set of particles with random initial positions and velocities in the search space, with each particle representing a possible solution.
- (2) Calculating the fitness value of each particle and evaluating the advantages and disadvantages of the solution according to the fitness value.
- (3) According to the historical and global optimal positions of particles, adjusting the velocity and position of each particle concerning the specific optimization formula.
- (4) Judging the fitness of the particles and outputting the optimal solution if it meets the termination condition; otherwise, returning to step (2) to continue the iteration.

2.2. SVM Method

Support Vector Machine is a supervised learning model proposed by Vapnik in 1995 [38]. The principle of SVM is shown in Figure 2. It is mainly used for classification and regression analysis. SVM classifies samples of different classes by constructing an optimal hyperplane. It has good generalization ability and is suitable for high-dimensional

and nonlinear datasets, especially in small samples and nonlinear problems. However, it has high computational complexity on large-scale datasets [39–41].

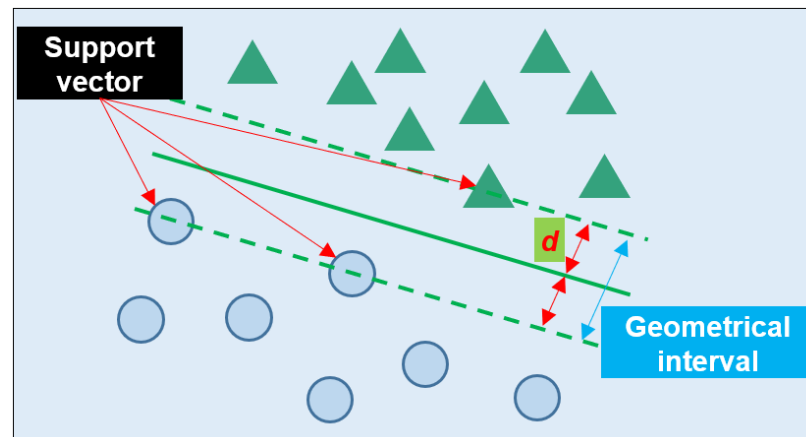


Figure 2. Schematic diagram of support vector machine.

The basic principles of SVM are as follows.

(1) Commonly used kernel functions include linear, polynomial and radial basis functions. The choice of kernel function significantly impacts the classification effect of SVM.

(2) A hyperplane that maximizes the classification interval is found by solving a constrained optimization problem.

(3) The optimal hyperplane is used to predict the classification or regression of new samples.

2.3. Inversion Steps of Rock Mechanical Parameters

Based on the engineering geological background and design scheme, the appropriate surrounding rock constitutive model, support constitutive model and boundary conditions are selected. The three-dimensional numerical model of the water diversion surge shaft is established by FLAC3D. According to the long-term monitoring data of the dome on site, the influence of each parameter on the maximum deformation is analyzed by SVM, the parameter selection is optimized and the parameter orthogonal analysis table is formulated. The in situ stress inversion is carried out for the monitoring and measurement of the displacement. The calculated displacement of the numerical model is compared to the monitored displacement to verify accuracy. Then, the deformation parameter database of the surrounding rock is established. After assigning initial values to rock mass parameters according to preliminary geological characteristics, the three-dimensional numerical model is excavated and supported in layers, and deformation characteristic data are recorded. Rock mechanical parameter inversion is performed through a particle swarm optimization–support vector machine algorithm. Through repeated updates and iterations, the minimum error value is continuously reduced until the accuracy requirements are met and the optimal value of the required parameter is obtained. Finally, assuming that the variability of rock mass parameters is relatively consistent, the excavation of the next layer is based on the rock mechanical parameters of that layer. The different support schemes are compared and analyzed, and the above steps are repeated until the excavation is completed. The inversion steps of rock mechanical parameters are shown in Figure 3.

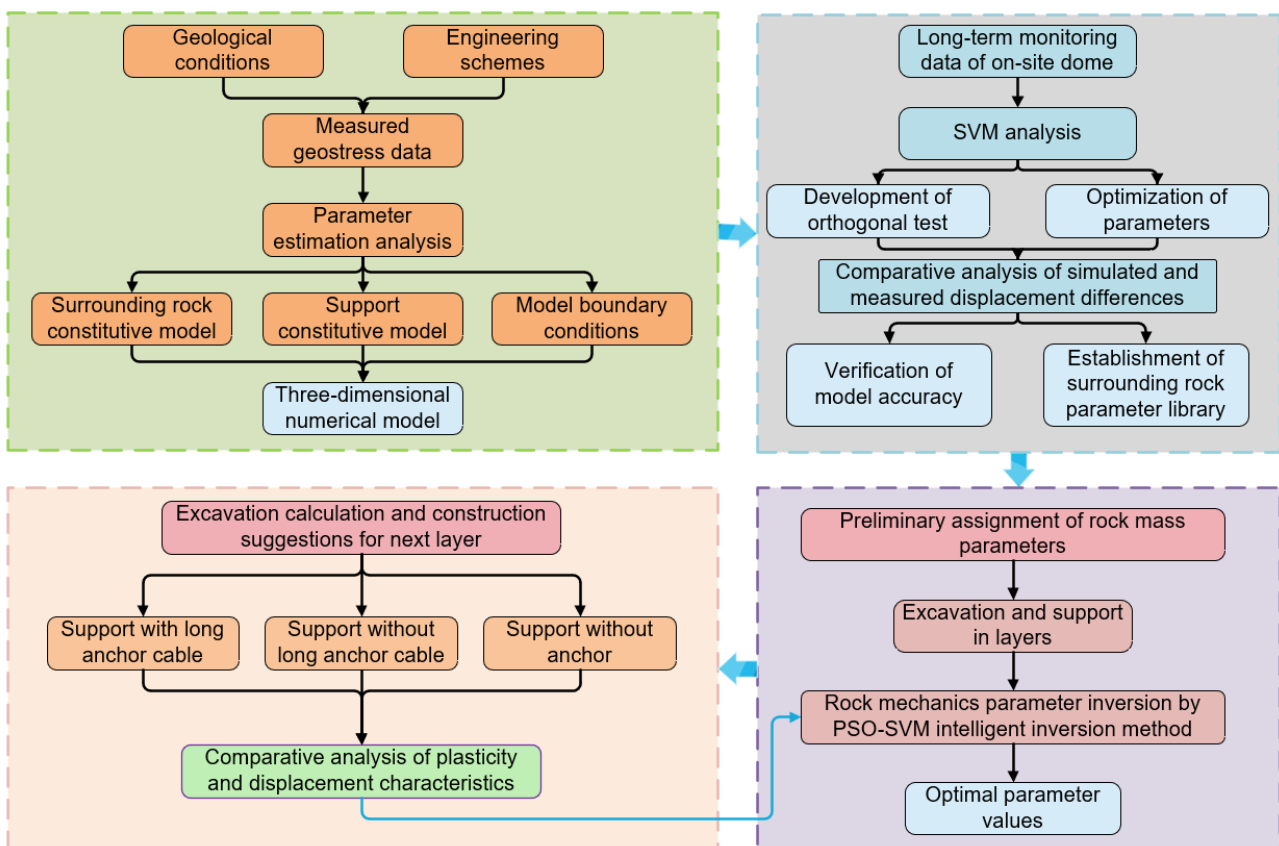


Figure 3. Inversion steps of rock mechanical parameters.

3. Inversion of Surrounding Rock Parameters of Water Diversion Surge Shaft

3.1. Engineering Situations

The shape of the water diversion surge shaft based on a water conservancy project is a circular impedance surge shaft. The dome height is 14 m, the maximum excavation diameter is 35 m, the excavation diameter of the shaft section is 33.40 m and the height is 79.50 m. The thickness of the overlying rock mass on the top arch of the surge shaft, which is constructed in the fine-grained biotite monzogranite of the Yanshanian period, is 135 m. Geological surveys and low-elevation exploration tunnels reveal that there are a small number of randomly developed NW-trending steeply dipping small faults or compressive fracture zones in the surrounding rock. The geological structure is mainly characterized by joint fissures. The weathering degree of rock mass is generally slightly weathered with four groups of dominant joints (N40°~60°W/SW(NE)∠60°~80°, N55°~80°E/SE∠65°~80°, SN/E∠60°~80°, N30°~45°W/SW(NE)∠10°~20°) whose spacing is large. The rock mass has good integrity and is characterized by numerous block and sub-block structures.

3.2. Construction of the Numerical Model

According to the layout of the surge chamber, the numerical model of the cavern is established by using the finite difference software FLAC3D V7.0 (Figure 4) to realize the dynamic simulation of excavation. According to the Saint Venant principle [42], to ensure that the initial stress state is always maintained around the model, the size of the model should be about three to five times the maximum size of the excavation object. Therefore, the transverse (X-axis direction) width of the model is 340 m, the longitudinal (Y-axis direction) width is 200 m and the height from the bottom to the arch bottom (Z-axis direction) is 190 m. The Shell element is employed to simulate the supporting structure, and the Cable element is used to simulate the steel bar, prestressed anchor cable, anchor bolt, etc. The total number of model elements is 3,078,024.

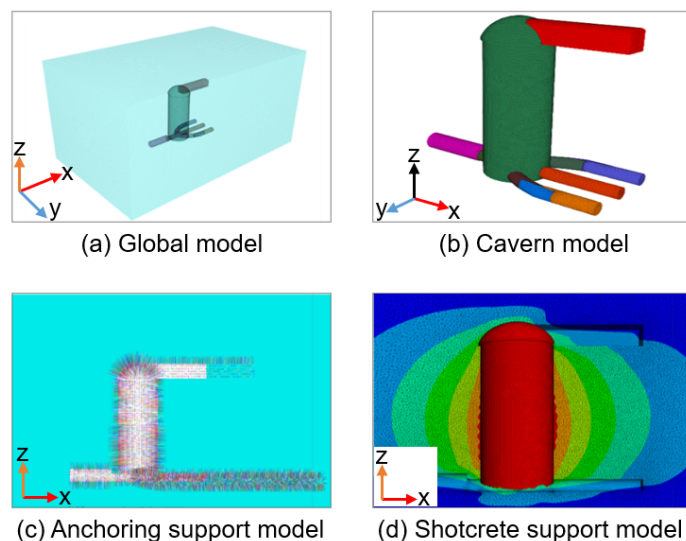


Figure 4. Numerical model.

3.3. Parameter Inversion Results

Based on the dome monitoring data, the parameter orthogonal test plan (Table 1) is developed, and the influence of each parameter on the maximum deformation is analyzed by SVM, optimizing the mechanical parameters. The analysis results shown in Figure 5 demonstrate that with the increase in cohesion, the upper limit of the maximum deformation of the surrounding rock remains unchanged, but the lower limit decreases. With the increase in the elastic modulus of the surrounding rock, the upper and lower limits of the maximum deformation of the surrounding rock decrease. The range of the maximum deformation of the surrounding rock increases with the increase in the surrounding rock parameters.

Table 1. Orthogonal analysis table of mechanical parameters.

Experiment Number	Elastic Modulus (GPa)	Internal Friction Angle (°)	Cohesive Force (MPa)	Maximum Deflection (mm)
0	20	45	3	4.73
1	15	35	2.5	5.41
2	20	40	3	4.5
3	25	45	3.5	3.11
4	15	40	3.5	5.69
5	20	45	2.5	5.01
6	25	35	3	3.22
7	15	45	3	5.22
8	20	35	3.5	4.17
9	25	40	2.5	3.8

By using the numerical simulation analysis method, the deformation characteristics of surrounding rock under different working conditions are obtained (Figure 6). Furthermore, the rock mechanical parameter inversion method based on the PSO-SVM algorithm (Figure 7) is employed to obtain the characteristics of rock mechanical parameters at an elevation of 2940 m, which demonstrates that the elastic modulus is 22 GPa, the internal friction angle is 43°, and the cohesion is 0.3 MPa. According to the assumption that the variability of rock parameters is minimal, the rock parameters obtained this time are used to guide the excavation of the cavern at the next elevation, and the rock mechanical parameters at the elevations of 2922 m and 2898 m are obtained by inversion. The inversion of surrounding rock at an elevation of 2922 m demonstrates that the elastic modulus is 23 GPa, the internal friction angle is 41° and the cohesion is 0.3 MPa. The inversion of surrounding

rock at an elevation of 2898 m demonstrates that the elastic modulus is 24 GPa, the internal friction angle is 43° and the cohesion is 0.4 MPa.

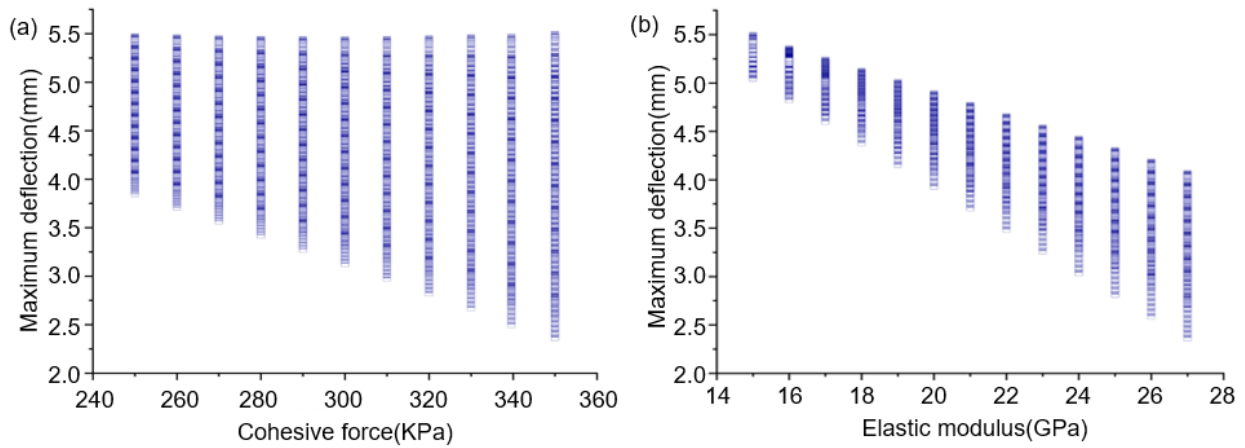


Figure 5. Influence of different mechanical parameters of surrounding rock on deformation: (a) The influence of cohesion of surrounding rock on deformation; (b) The influence of elastic of surrounding rock on deformation.

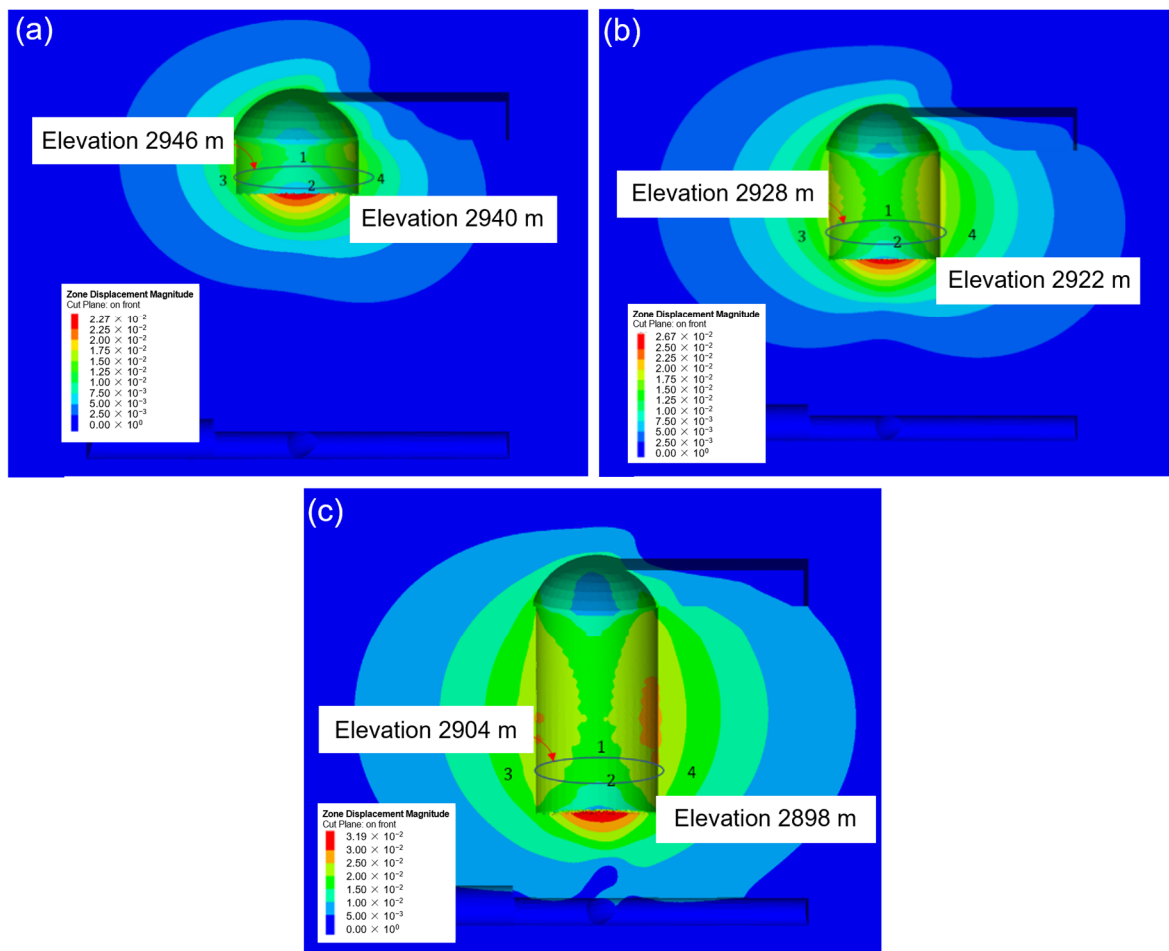


Figure 6. Deformation characteristics of surrounding rock under different working conditions: (a) elevation 2940 m; (b) elevation 2922 m; (c) elevation 2898 m. (the numbers 1–4 are the scheduled installation positions of the multipoint displacement meters).

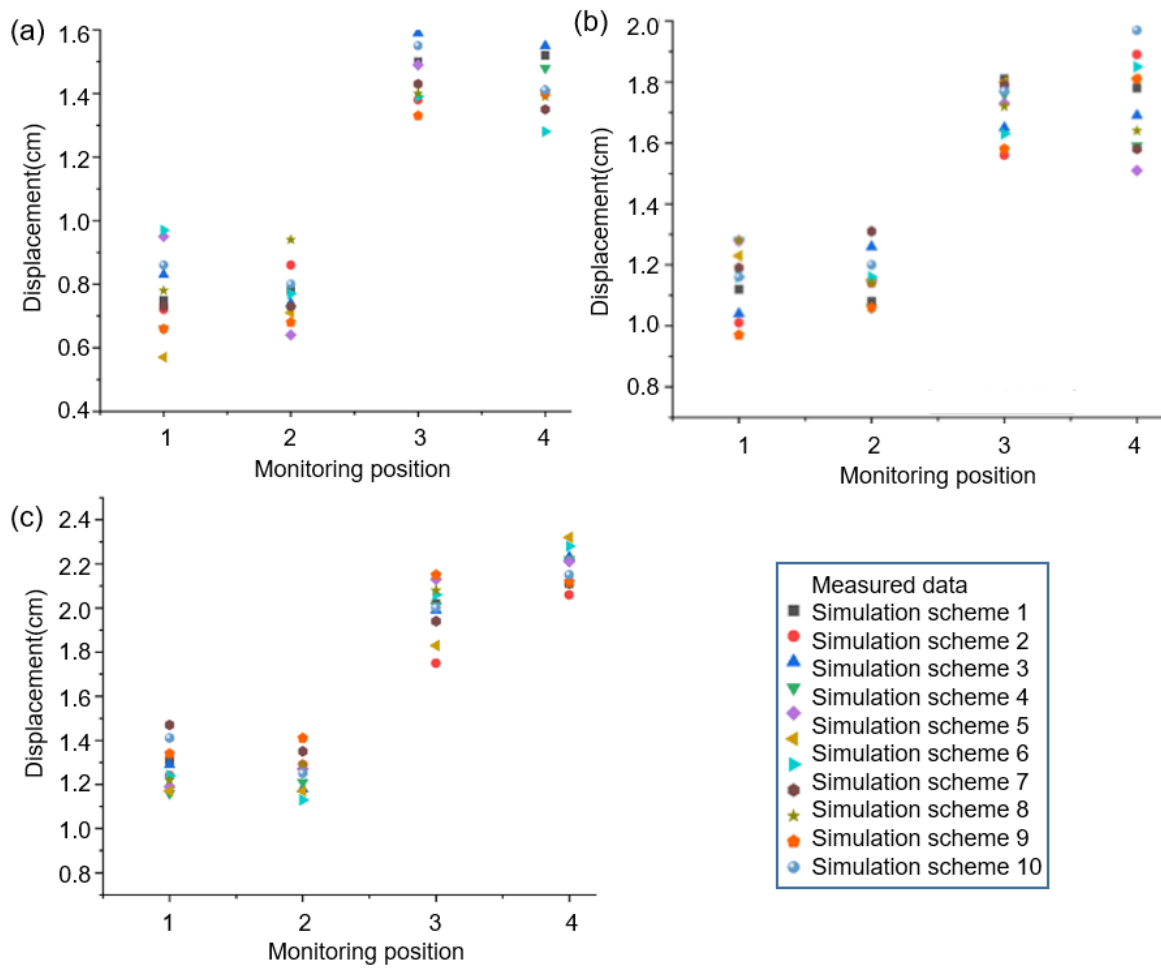


Figure 7. PSO-SVM parameter inversion: (a) elevation 2940 m; (b) elevation 2922 m; (c) elevation 2898 m.

3.4. Comparison of Field Monitoring Data and Numerical Simulation Results

Multi-point displacement meters are installed on the profile near an elevation of 2926 m. Taking the deepest point of the anchor head as the relatively fixed point, the absolute displacement values of the surface, depth 10 m and depth 5 m, are calculated. Its location, number and installation process are shown in Figure 8.

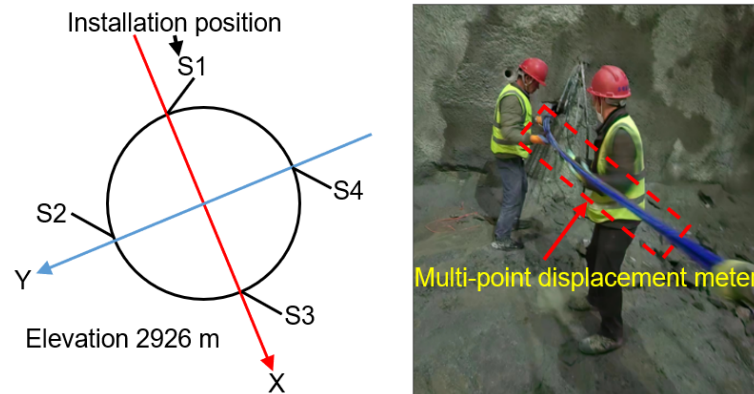


Figure 8. Installing a multi-point displacement meter.

To verify the accuracy of the numerical model, the absolute displacement–time diagram is drawn based on the displacement data (Figure 9). As shown in Figure 9, during the monitoring period, the overall temperature change is relatively gentle and without sudden changes. The average temperature change in the first two weeks is 0.39 °C per day, so the impact on the displacement monitoring of each anchor head is negligible.

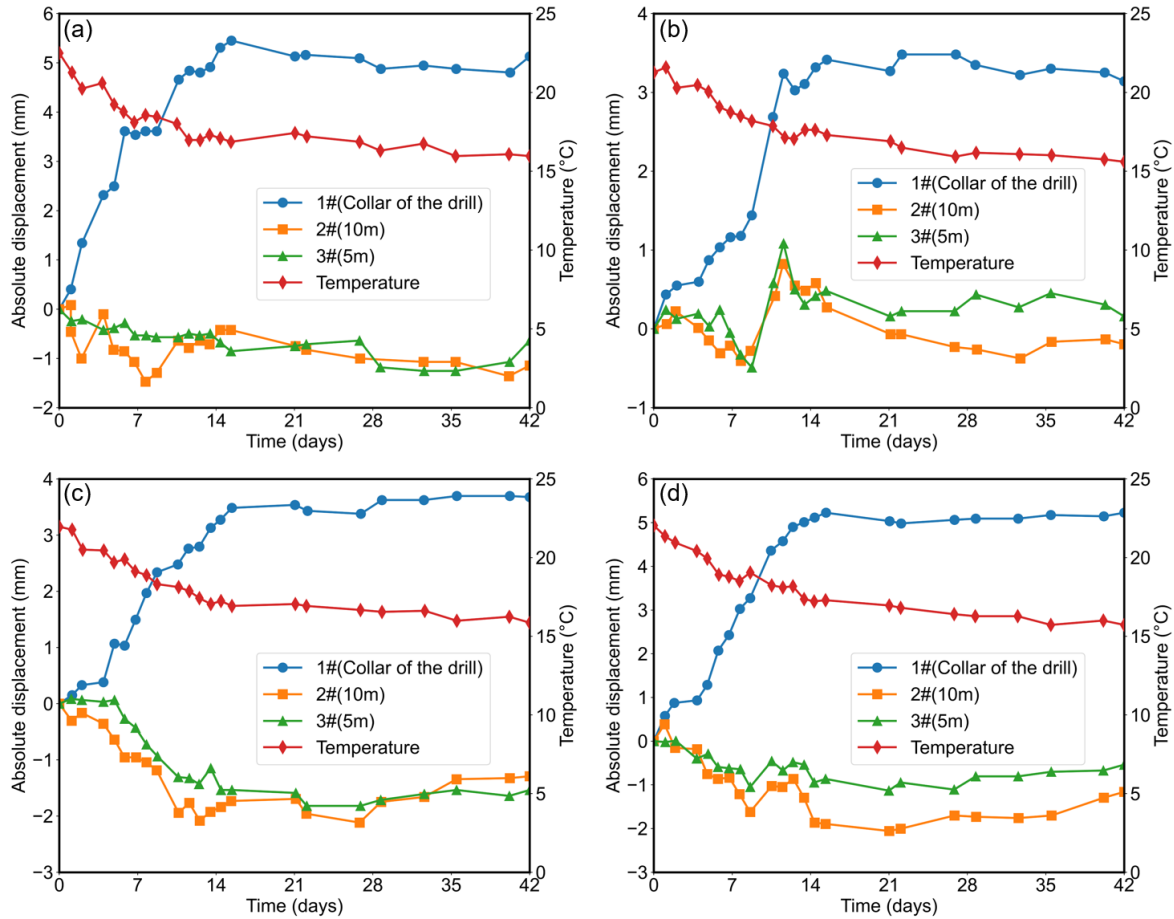


Figure 9. Absolute displacement–time diagram: (a) S1; (b) S2; (c) S3; (d) S4.

The absolute displacement values of the 1# anchor heads of each multi-point displacement meter showed a trend of increasing first and then stabilizing, among which S1-1# reached a maximum value of 5.4 mm on the sixteenth day, S2-1# reached a maximum value of 3.47 mm on the twenty-third day, S3-1# reached a maximum value of 3.71 mm on the thirty-seventh day and S4-1# reached a maximum value of 5.32 mm on the forty-second day. Except for the S2-2# and S2-3# anchor heads, the absolute displacement values of the 2# and 3# anchor heads of the other multi-point displacement meters also showed a trend of first decreasing and then tending to be stable. During the second week of monitoring, the sudden increase in the absolute displacement values of each S2 anchor head may be related to the heterogeneity of the surrounding rock. Since the elastic modulus of the surrounding rock in the buried direction of the S2 multi-point displacement meter is relatively high, the surrounding rock only has surface displacement in the early stage of excavation. As the distance between the surface and the depth of the surrounding rock increases, the tensile stress on the surrounding rock also increases. Eventually, the rock is destroyed, and the absolute displacement of each anchor head increases accordingly.

Based on the measured displacement data recorded by the multi-point displacement meter, the maximum relative displacements between the surface of the cavern monitored by S1, S2, S3 and S4 and the depth of 10 m are calculated, which are 3.6 mm, 5.0 mm, 6.0 mm

and 6.7 mm, respectively, with an average maximum relative displacement of 5.32 mm. As shown in Figure 10, the displacement of the surrounding rock on the surface of the cave is about 22.0 mm, and the displacement of the deep surrounding rock at 10 m is 17.5 mm, resulting in a relative displacement of 4.5 mm. The numerical simulation results of the relative displacement of the surrounding rock are compared with the average value of the measured results; the difference between them is 1.82 mm, indicating that the numerical simulation results are consistent with the measured results and proving that the numerical model has high accuracy.

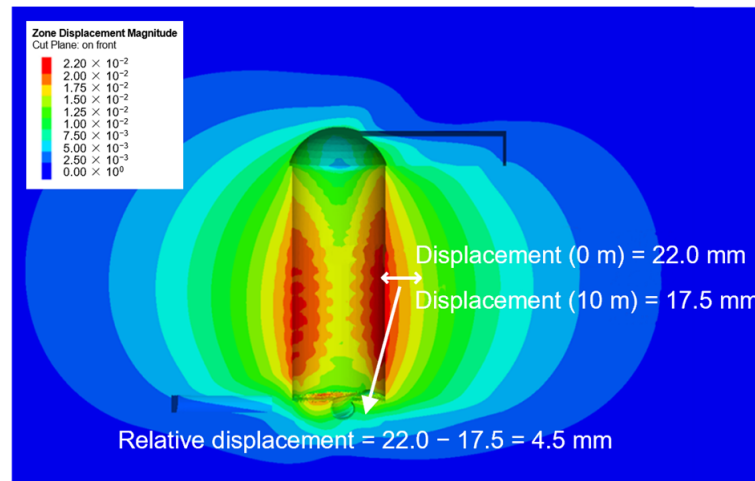


Figure 10. Displacement of water diversion surge shaft in numerical simulation.

4. Analysis of Deformation Characteristics of Water Diversion Surge Shaft Under Different Supports During Layered Excavation

According to the construction documents, the water diversion surge shaft is excavated in layers. The profile of the support scheme along the water flow direction is shown in Figure 11. (The red lines in the figure are long anchor cables that form an angle of 15° with the horizontal plane. They are arranged in five rows at an elevation of 2916 to 2891, with 17 cables in each row and a row spacing of 6 m. The short anchor bolts are shown in the subsequent support schemes.) The support schemes in different elevations are shown in Figure 12. A numerical simulation support model is established based on the support schemes (Figure 13).

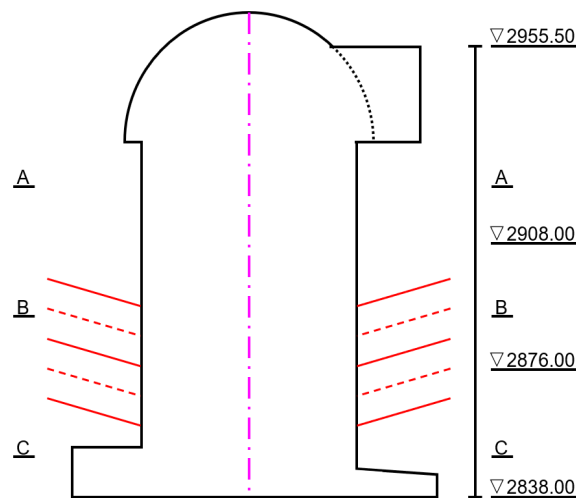


Figure 11. Profile of the support scheme along the water flow direction. (A, B, C are marks for dividing the general position profile of the water diversion surge shaft).

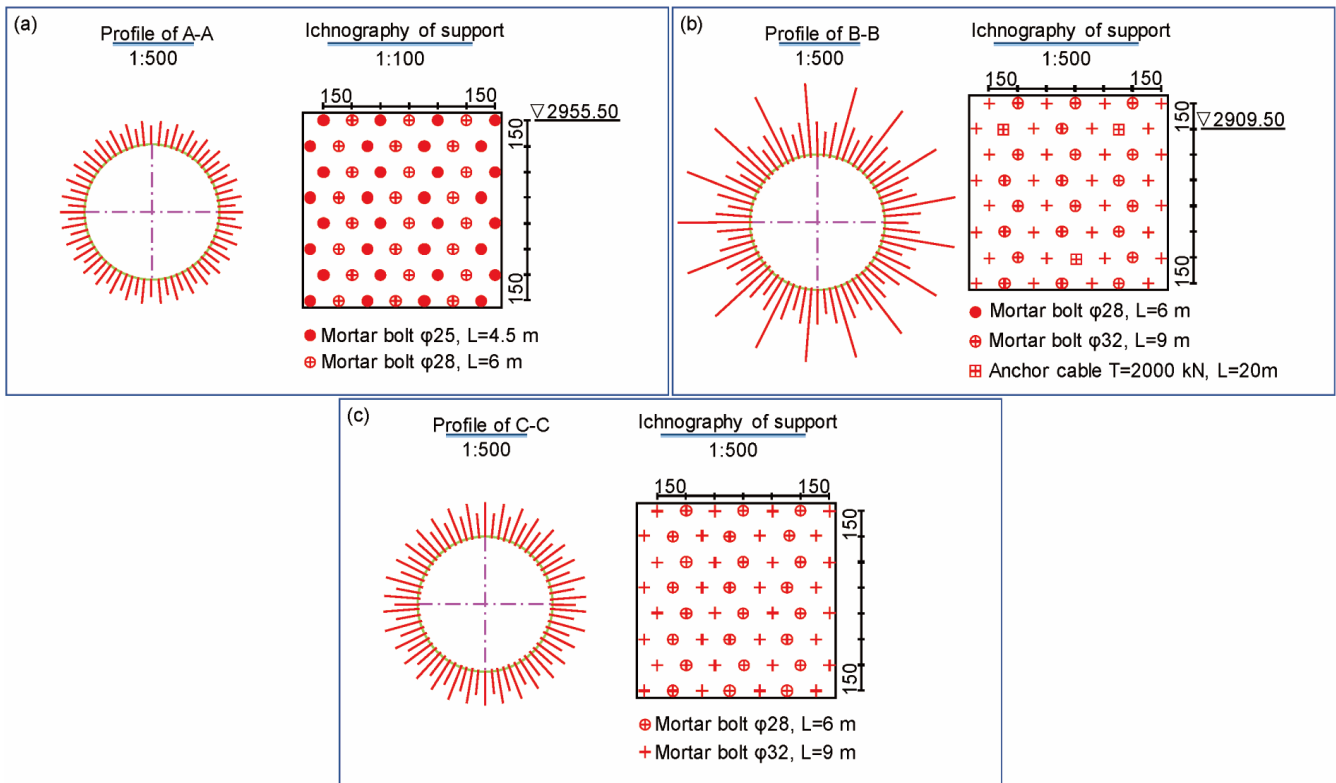


Figure 12. Support schemes in different elevations: (a) 2916~2955 m; (b) 2890~2916 m; (c) 2876~2890 m.

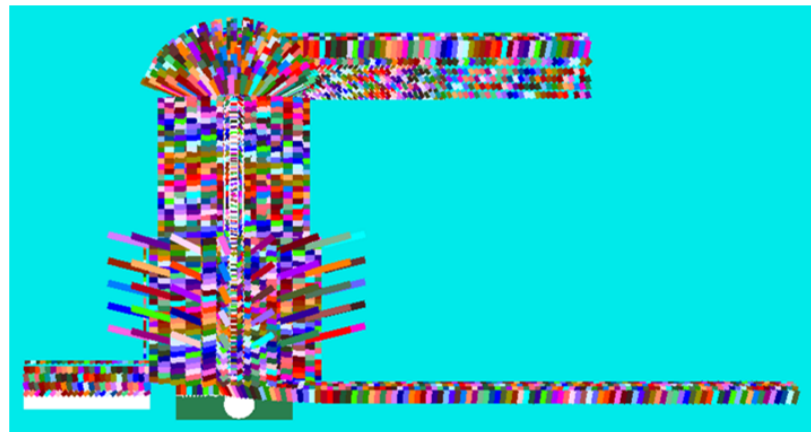


Figure 13. Profile of the support scheme of the numerical simulation.

To study the differences between different support schemes, the deformation characteristics of the water diversion surge shaft under the conditions of support with a long anchor cable, support without a long anchor cable and support without an anchor are analyzed based on FLAC3D. The research results are shown in Figures 14–16. By comparing Figures 14–16, it is found that when the excavation depth is small, the maximum displacement of the surge shaft mainly occurs in the middle part directly below the excavation area. As the excavation depth increases, the maximum displacement of the side walls on both sides of the water diversion surge shaft and the depth of the plastic zone increases significantly, and the failure form of the plastic zone is mainly shear failure.

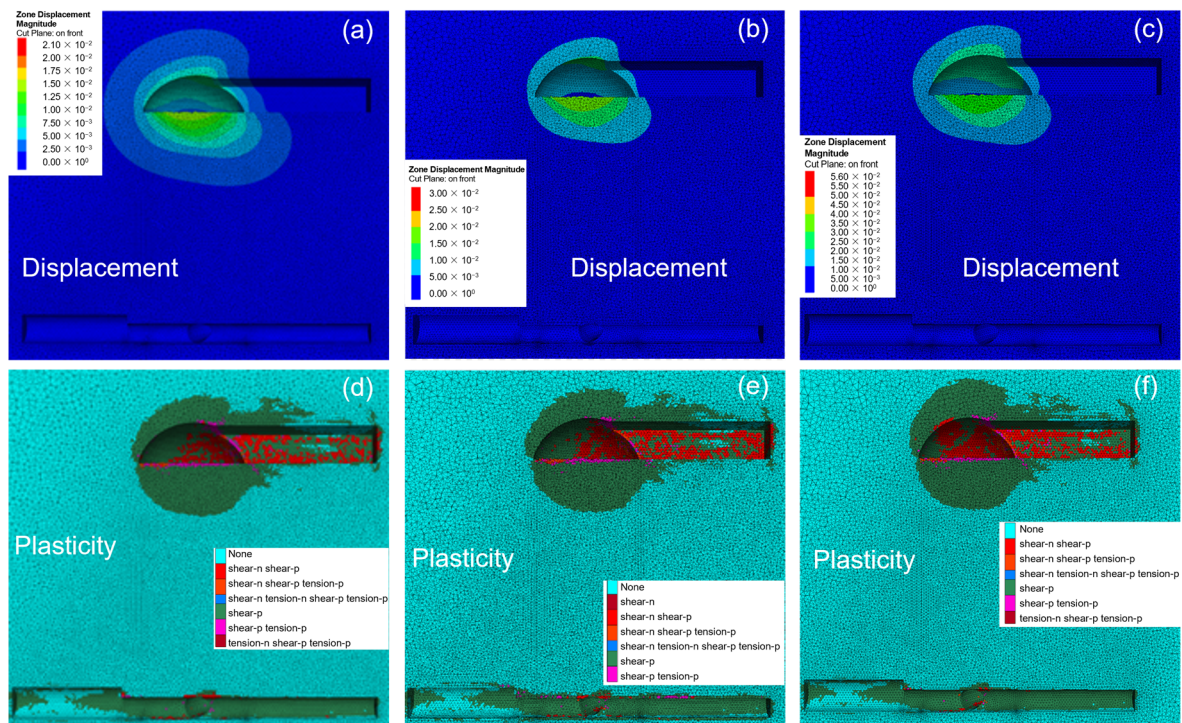


Figure 14. Displacement and plastic characteristics of water diversion surge shaft in the dome: (a) support with long anchor cable; (b) support without long anchor cable; (c) support without anchor; (d) support with long anchor cable; (e) support without long anchor cable; (f) support without anchor.

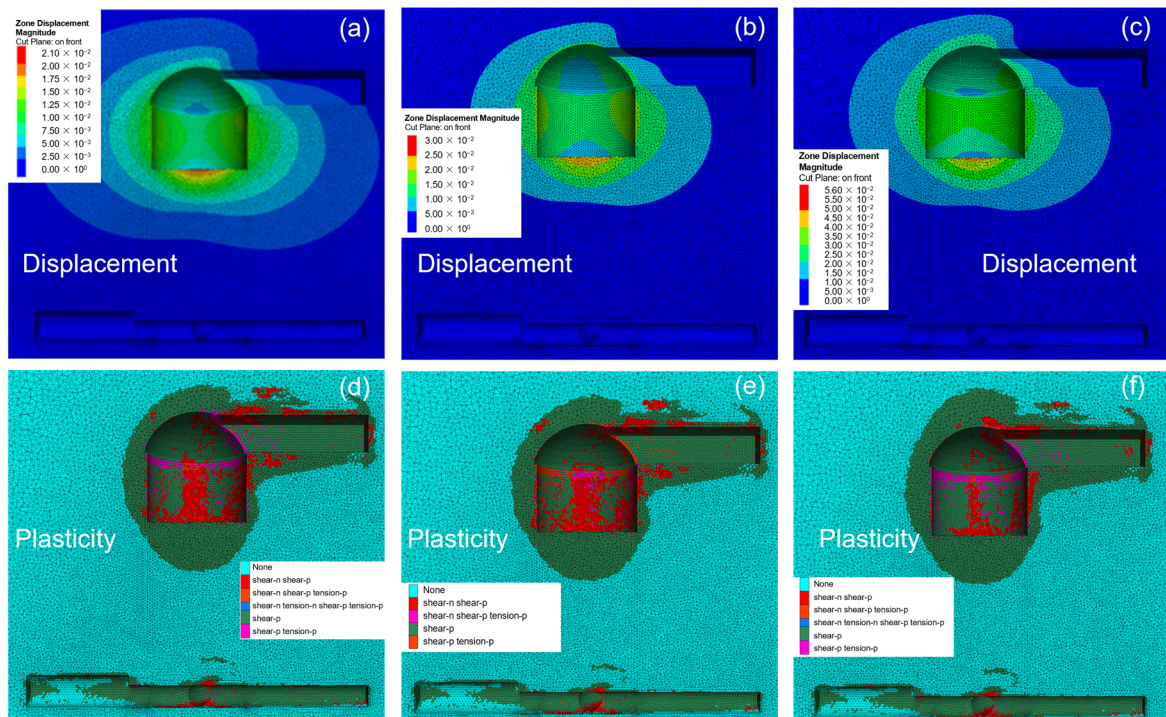


Figure 15. Displacement and plastic characteristics of water diversion surge shaft in elevation 2931: (a) support with long anchor cable; (b) support without long anchor cable; (c) support without anchor; (d) support with long anchor cable; (e) support without long anchor cable; (f) support without anchor.

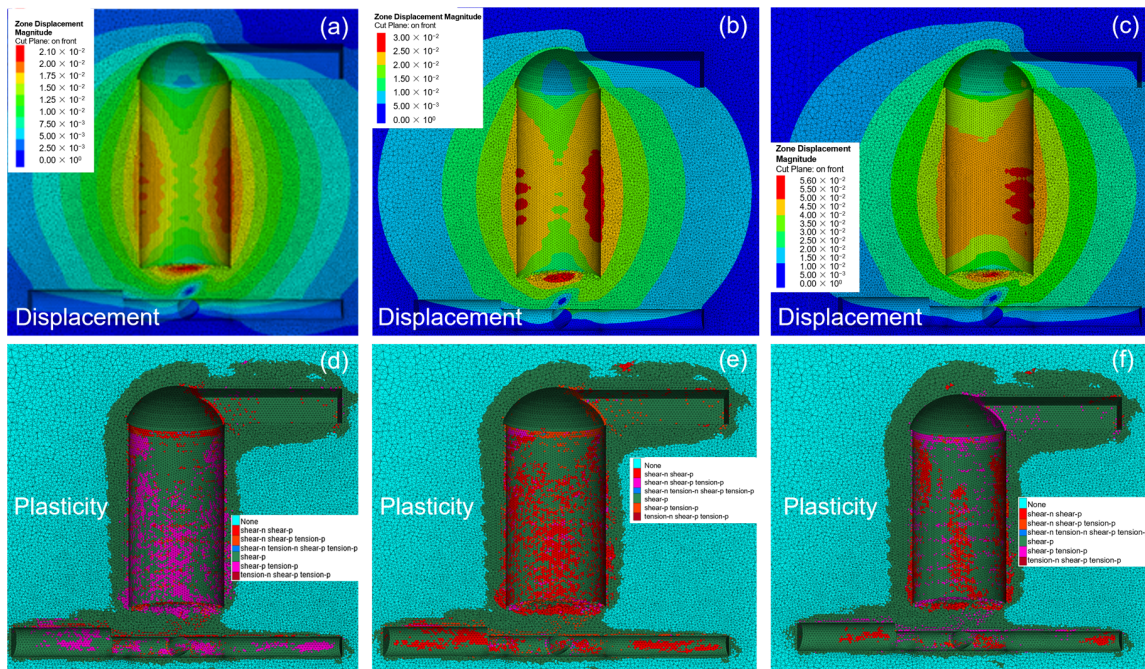


Figure 16. Displacement and plastic characteristics of water diversion surge shaft in elevation 2886: (a) support with long anchor cable; (b) support without long anchor cable; (c) support without anchor; (d) support with long anchor cable; (e) support without long anchor cable; (f) support without anchor.

According to the displacement characteristics, before excavation at the elevation of 2931 m, the interaction between the lower tunnel and the water diversion surge shaft is weak. When excavated to the elevation of 2886 m, the interaction between the lower tunnel and the water diversion surge shaft is greatly intensified, and attention should be paid to observing the stability of the lower cavern. The influence on the dome is relatively weak during the increase in excavation depth. After excavation at an elevation of 2886 m, under the action of the extended anchor cable, the displacement of the side walls on both sides of the water diversion surge shaft is relatively uniform, and the displacement on the right side is slightly larger than that on the left side. Without the long anchor cable support, the unevenness of the displacement of the side walls on both sides becomes more obvious, and the displacement field is connected in the middle of the water diversion surge shaft. Without anchor support, the displacement of the right side wall is significantly greater than that of the left side. The support effect of the left support device is weak. The right side wall displacement should be paid special attention to, and corresponding support measures should be set up. Regarding the plastic characteristics, before excavation at the elevation of 2886, there is no significant difference in the plastic zone under the effect of the support with long anchor cables and the support without long anchor cables. When excavating the dome, the shear failure plastic zone is concentrated on the right side of the dome. When excavating to the 2931 elevation, the plastic zone is concentrated in the middle of the surge shaft.

When comparing the displacement and plastic characteristics of the water diversion surge shaft excavation process under three support schemes, it is evident that with anchor support, the surrounding rock is influenced by the combined action of anchor bolts/cables and shotcrete. This increases overall stability and effectively controls displacement and deformation, resulting in a relatively uniform stress distribution area between the rock mass and the support structure. Compared with the surrounding rock supported without long anchors, the surrounding rock supported with long anchors has a smaller overall displacement and significantly reduced plastic zone area. Compared with the surrounding rock without anchor support, the surrounding rock with anchor support has improved overall bearing capacity and a significantly reduced plastic zone area under the tension of anchor bolts/cables and the constraint of shotcrete, thus reducing plastic deformation.

5. Response Characteristics of Surrounding Rock of Water Diversion Surge Shaft at the Excavation Completion Stage Under Different Support Schemes

After the completion of excavation in the water diversion surge shaft, the comprehensive response characteristics of the surrounding rock under different support schemes need to be further studied. FLAC3D is used to establish three-dimensional numerical models of the schemes of support with long anchor cables, support without long anchor cables, and support without anchor. The displacement and plastic zone characteristics of the surrounding rock at the excavation completion stage under different support schemes are compared and analyzed under the maximum principal stress and the minimum principal stress.

5.1. Comparative Analysis of Surrounding Rock Displacement of Water Diversion Surge Shaft Under Different Support Schemes

As shown in Figure 17, in the direction of maximum principal stress, under the influence of ground stress and excavation disturbance, the maximum deformation of the surrounding rock under the long anchor cable support is 2.15 cm, and the maximum deformation of the surrounding rock after the long anchor cable is removed is 2.75 cm. The maximum deformation of the surrounding rock under no anchor support is 6.22 cm. Compared with the scheme of support without long anchor cables, the maximum deformation of the surrounding rock under no anchor support increases significantly, with an increase of 3.47 cm. In the direction of minimum principal stress, the maximum deformation of the surrounding rock under each support scheme is smaller than the maximum deformation of the surrounding rock in the direction of maximum principal stress. The maximum deformation of the surrounding rock under support with long anchor cables is 2.0 cm, and the maximum deformation of the surrounding rock under support without long anchor cables is 2.25 cm. The maximum deformation of the surrounding rock without anchor support is 6.1 cm, which increases by 3.85 cm compared with the support without long anchor cables. The surrounding rock deformation degree of each support scheme shows a trend of increasing first and then decreasing with increasing depth, and the maximum surrounding rock deformation occurs in the middle and lower sections of the surge shaft. After comparison, the support with long anchor cables has the best control effect on the surrounding rock displacement, followed by the support without long anchor cables, and the support without an anchor cannot effectively control the surrounding rock displacement. Comparing Figure 17a,b, it can be seen that the displacement of the surrounding rock in the direction of the maximum principal stress is greater than the displacement of the surrounding rock in the direction of the minimum principal stress. To prevent the instability of the surge shaft, the displacement of the surrounding rock in the direction of the maximum principal stress should be focused on according to the displacement characteristics.

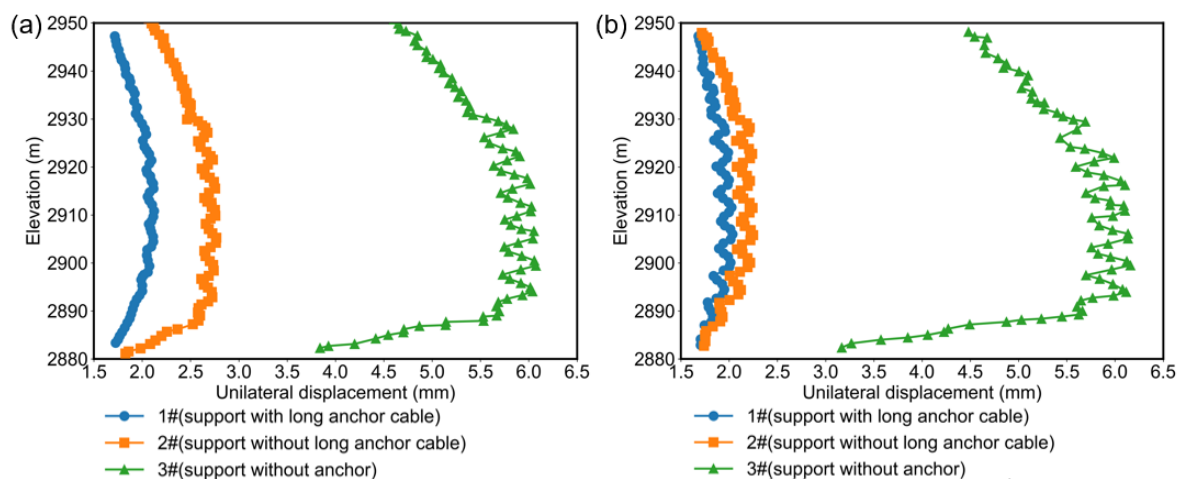


Figure 17. Displacement characteristics under different elevations: (a) maximum principal stress direction; (b) minimum principal stress direction.

5.2. Comparative Analysis of Plastic Zone of Surrounding Rock of Water Diversion Surge Shaft Under Different Support Schemes

As shown in Figure 18, in the direction of maximum principal stress, the maximum depth of the plastic zone under the support with long anchor cables is 5.3 m. Under the support without long anchor cables, the maximum depth of the plastic zone is 6.6 m. The maximum depth of the plastic zone without anchor support is 7.9 m, which is 1.3 m higher than that without long anchor support. As shown in Figure 19, in the direction of minimum principal stress, the maximum depth of the plastic zone is 16.2 m under the effect of the support with long anchor cables, and the maximum depth of the plastic zone is 18.6 m under the support without long anchor cables. The maximum depth of the plastic zone without anchor support is 21.2 m, and the depth of the plastic zone increases by 2.6 m compared with the support without long anchor cables. The plastic zones of the three surrounding rocks are mainly shear failure. It can be seen that the surge shaft has been in a high-stress environment, and the excavation leads to various plastic states, resulting in the instability of the surrounding rock damage. The plastic zone in the direction of the minimum principal stress is much larger than that in the direction of the maximum principal stress. Especially in the absence of long anchor cable support or anchorless support, the plastic zone spreads to the entire surge shaft. To ensure the stability of the surge shaft, the support with long anchor cables is essential and the plastic deformation in the direction of the minimum principal stress should be focused on.

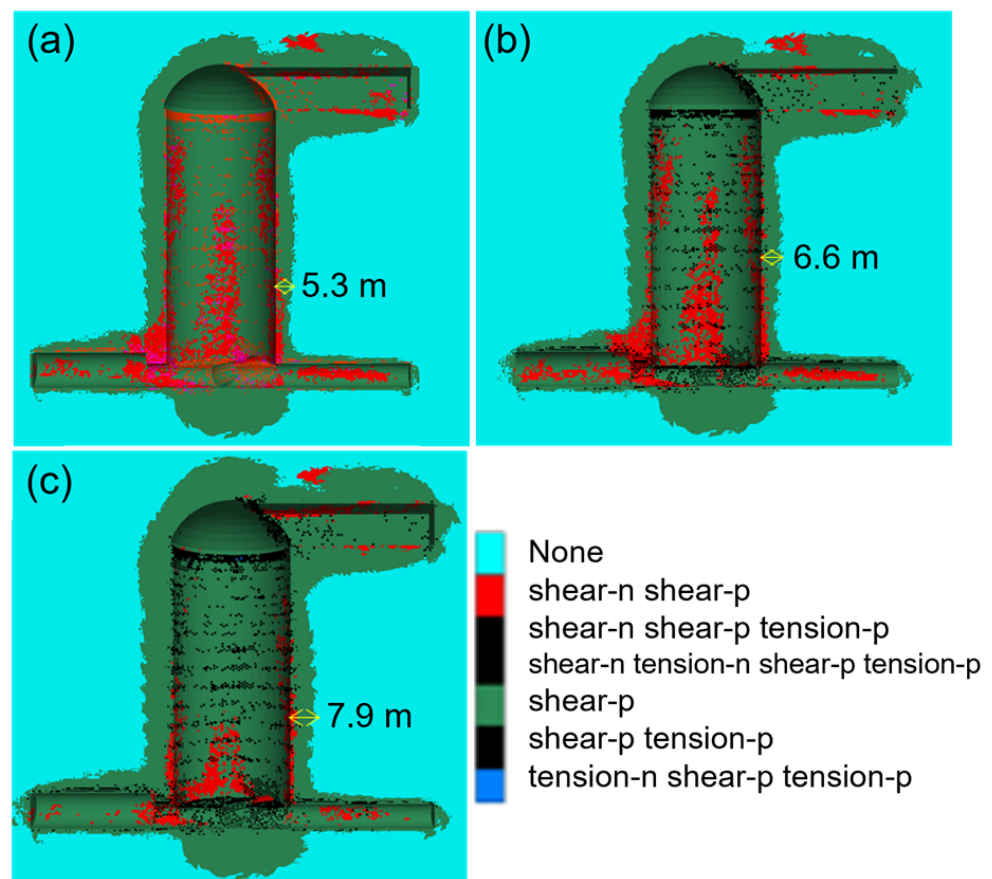


Figure 18. Plastic characteristics of maximum principal stress direction: (a) support with long anchor cable; (b) support without long anchor cable; (c) support without anchor cable.

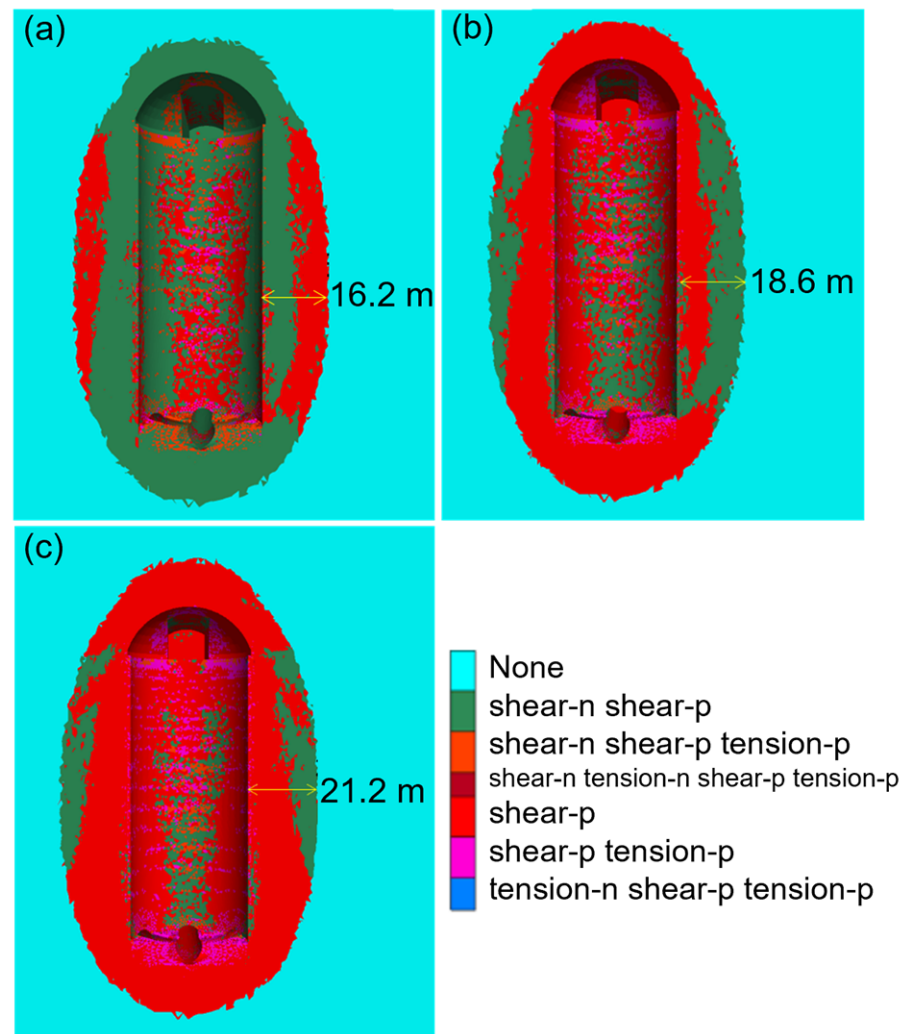


Figure 19. Plastic characteristics of minimum principal stress direction: (a) support with long anchor cable; (b) support without long anchor cable; (c) support without anchor cable.

6. Conclusions

In this paper, a PSO-SVM surrounding rock mechanical parameter inversion algorithm is established according to the geological conditions and monitoring data of a water diversion surge shaft excavation project. Based on the SVM-PSO intelligent inversion algorithm, the surrounding rock mechanical parameters are obtained. Using three-dimensional numerical simulation software, the displacement and plasticity characteristics of the surrounding rock during the excavation of the water diversion surge shaft are analyzed. The following conclusions are drawn:

(1) A rock mechanical parameter inversion method is proposed, combining particle swarm optimization and support vector machine. An orthogonal analysis is conducted on monitoring data to establish a database of surrounding rock mechanical parameters. The particle swarm optimization is employed to globally search for and optimize these parameters. Finally, the support vector machine is applied to perform local refined fitting, which effectively enhances the accuracy and efficiency of the parameter inversion process.

(2) By analyzing the plastic zone and displacement field of the surrounding rock under the layered excavation, it is found that the main form of destruction of the plastic zone of the surrounding rock is shear failure. With the increase in excavation depth, the support from the upper surrounding rock decreases, increasing the stress of the lower surrounding rock. The surrounding rock after stress redistribution produces the maximum deformation in the middle and lower parts. Therefore, special attention should be paid to the shear failure

area of the surrounding rock and the deformation of the middle and lower surrounding rock during the excavation, taking corresponding support measures.

(3) After excavation, in the maximum principal stress direction, compared with the long anchor cable support, the deformation increased by 0.6 cm under the support without long anchor cables, and the deformation increased by 4.07 cm without anchor support. In the minimum principal stress direction, compared with the long anchor cable support, the deformation increased by 0.25 cm under the support without long anchor cables, and the deformation increased by 3.99 cm without anchor support. In the maximum principal stress direction, compared with the support with long anchor cables, the plastic zone depth increased by 1.3 m under the support without long anchor cables. In the minimum principal stress direction, compared with the long anchor cable support, the plastic zone depth increased by 2.4 m under the support without long anchor cables. In terms of controlling the deformation of the surrounding rock and limiting the development of the plastic zone, the support with long anchor cables is significantly better than the support without long anchor cables.

(4) Complex geological conditions will inevitably be encountered during the construction process. Taking into account the variability of surrounding rock parameters, how to invert the mechanical parameters of expansive soft rock, a rock mass that is strongly affected by hydraulic properties, will become the focus of our subsequent research.

Author Contributions: Conceptualization, X.-W.Z. and G.L.; methodology, X.-W.Z.; software, T.Z.; validation, X.-W.Z., T.Z., G.L., Y.H., B.D. and T.Y.; formal analysis, X.-W.Z. and Y.H.; investigation, X.-W.Z. and B.D.; resources, G.L.; data curation, X.-W.Z.; writing—original draft preparation, X.-W.Z., T.Z., G.L., Y.H. and T.Y.; writing—review and editing, G.L. and Y.H.; visualization, X.-W.Z. and Y.H.; supervision, G.L. and B.D.; project administration, G.L.; funding acquisition, G.L. All authors have read and agreed to the published version of the manuscript.

Funding: The research was funded by the Zhejiang Provincial Natural Science Foundation (LQ24D020001), the open Fund of State Key Laboratory of High-speed Railway Track Technology (2022YJ127-1) and the Open Project of Key Laboratory of Geotechnical and Underground Engineering of the Ministry of Education (Tongji University) (KLE-TJGE-B2306).

Data Availability Statement: Data are contained within the article.

Acknowledgments: Thanks to the help of three anonymous reviewers and journal editors.

Conflicts of Interest: Xing-Wei Zou was employed by the Sino-Hydro Bureau 5 Co., Ltd. The remaining authors declare that the research was conducted in the absence of any commercial or financial relationships that could be construed as a potential conflict of interest.

References

- Li, X.; Wang, H.; Jia, J.; Yang, C.; Hu, G.; Xue, Z. Ultimate displacement discrimination of stability and reliability analysis of surrounding rocks of tunnel and underground engineering. *Rock. Soil. Mech.* **2005**, *26*, 850–854.
- Xie, G.; Li, C.; Wang, L. Mechanical characteristics and practical application on stress shell of roadway surrounding rock. *J. China Coal Soc.* **2016**, *41*, 2986–2992.
- Fu, Q.; Yang, J.; Gao, Y.B.; Li, C.J.; Song, H.X.; Liu, Y.X.; Wu, X. Combined blasting for protection of gob-side roadway with thick and hard roof. *J. Rock. Mech. Geotech.* **2024**, *16*, 3165–3180. [[CrossRef](#)]
- Ren, F.Q.; Zhu, C.; Karakus, M.; He, M.C. Rockburst mitigation mechanisms of pressure relief borehole and rock bolt support: Insights from granite true triaxial unloading rockburst tests. *Eng. Geol.* **2024**, *336*, 107571. [[CrossRef](#)]
- Zhu, C.; Xing, X.S.; He, M.C.; Tang, Z.C.; Xiong, F.; Ye, Z.Y.; Xu, C.S. Failure behavior and strength model of blocky rock mass with and without rockbolts. *Int. J. Min. Sci. Technol.* **2024**, *34*, 747–762. [[CrossRef](#)]
- Xu, C.; Ren, Q.; Li, R. Entropy catastrophe criterion of surrounding rock stability. *Chin. J. Rock. Mech. Eng.* **2004**, *23*, 1992–1995.
- Zhao, S.J.; Zhang, Q.; Miao, Y.S.; Zhang, W.Z.; Zhao, X.B.; Xu, W. Sub-Homogeneous peridynamic model for fracture and failure analysis of roadway surrounding rock. *Cmes-Comp. Model. Eng.* **2024**, *139*, 3167–3187. [[CrossRef](#)]
- Zhou, P.; Shen, Y.; Zhao, J.; Zhang, X.; Gao, B.; Zhu, S. Research on disaster-induced mechanism of tunnels with steeply dipping phyllite strata based on an improved ubiquitous-joint constitutive model. *Chin. J. Rock. Mech. Eng.* **2019**, *38*, 1870–1883.
- Cheng, Q.; Guo, X. Study on comprehensive selection of mechanical parameters of rock mass in deep-buried tunnel anchor. *Chin. J. Undergr. Space Eng.* **2021**, *17*, 479–487.

10. Gao, M.; Ye, S.; Yang, B.; Liu, Y.; Li, J.; Liu, J.; Xie, H. Progress in research on deep in situ rock mechanics. *Bull. Natl. Nat. Sci. Found. China* **2021**, *35*, 895–903.
11. Xu, J.C.; Yang, C.B. Probabilistic back analysis based on adam, bayesian and multi-output gaussian process for deep soft-rock tunnel. *Rock Mech. Rock Eng.* **2023**, *56*, 6843–6853. [[CrossRef](#)]
12. Sun, J.L.; Wu, S.C.; Wang, H.; Wang, T.; Geng, X.J.; Zhang, Y.J. Inversion of surrounding rock mechanical parameters in a soft rock tunnel based on a hybrid model eo-lightGBM. *Rock. Mech. Rock. Eng.* **2023**, *56*, 6691–6707. [[CrossRef](#)]
13. Peng, Z.; Wang, Z.; Hong, C.; Li, K.; Li, A. Influence of parameter uncertainty on stability of underground water-sealed cavern. *J. Shandong Univ. Eng. Sci.* **2024**, *54*, 126–135.
14. Li, S.B.; Zhang, Y.G.; Cao, M.Y.; Wang, Z.N. Study on excavation sequence of pilot tunnels for a rectangular tunnel using numerical simulation and field monitoring method. *Rock. Mech. Rock. Eng.* **2022**, *55*, 3507–3523. [[CrossRef](#)]
15. Luo, Y.B.; Chen, J.X.; Chen, Y.; Diao, P.S.; Qiao, X. Longitudinal deformation profile of a tunnel in weak rock mass by using the back analysis method. *Tunn. Undergr. Sp. Tech.* **2018**, *71*, 478–493. [[CrossRef](#)]
16. Qin, S.L.; Zhao, X.D.; Song, J.Y.; Wang, C. Mechanical mechanism and theoretical analysis of anchor net support based on model test and numerical simulation. *Geomat. Nat. Haz Risk* **2024**, *15*, 2350484. [[CrossRef](#)]
17. Li, H.B.; Pan, W.P.; Hua, X.Z.; Luan, B.; Huang, Z.J. Instability characteristics of surrounding rock and surrounding rock control technology of deep coal roadway crossing the fault: A case study of Zhuxianzhuang coal mine. *Geomat. Nat. Haz Risk* **2024**, *15*, 2366376. [[CrossRef](#)]
18. Zhu, C.; He, M.C.; Karakus, M.; Zhang, X.H.; Tao, Z.G. Numerical simulations of the failure process of anacinal slope physical model and control mechanism of negative Poisson's ratio cable. *Bull. Eng. Geol. Environ.* **2021**, *80*, 3365–3380. [[CrossRef](#)]
19. Zhang, J.L.; Mei, M.; Wang, J.; Shang, G.P.; Hu, X.F.; Yan, J.; Fang, Q.; Plebankiewicz, E. The construction and application of a deep learning-based primary support deformation prediction model for large cross-section tunnels. *Appl. Sci.* **2024**, *14*, 912. [[CrossRef](#)]
20. Liu, L.; Li, T.B.; Ma, C.C. Research on 3D geological modeling method based on deep neural networks for drilling data. *Appl. Sci-Basel.* **2024**, *14*, 423. [[CrossRef](#)]
21. Mei, H.; Wang, Q.Y.; Yu, L.; Zeng, Q. A deep learning-based algorithm for intelligent prediction of adverse geologic bodies in tunnels. *Meas. Sci. Technol.* **2024**, *35*, 096119. [[CrossRef](#)]
22. Zhang, J.W.; Han, S.; Li, M.C.; Li, H.; Zhao, W.C.; Wang, J.; Liang, H. CasMDN: A deep learning-based multivariate distribution modelling approach and its application in geotechnical engineering. *Comput. Geotech.* **2024**, *168*, 106164. [[CrossRef](#)]
23. Zhou, Z.Q.; Bai, S.S.; Chu, K.W.; Li, J.L.; Sun, J.W.; Wang, M.X.; Sun, Y.; Li, M.H.; Liu, Y.H. Calibration of DEM macro and micro parameters via XGBoost method. *Granul. Matter.* **2022**, *24*, 106. [[CrossRef](#)]
24. Yang, W.; Zhang, Q.; Li, S.; Wang, G.; Li, Y. Application of particle swarm optimization in time-dependent parameters inversion. *J. Cent. South Univ. Sci. Technol.* **2013**, *44*, 282–288.
25. Ruan, Y.; Gao, C.; Liu, K.; Jia, R.; Ding, H. Inversion of rock and soil mechanics parameters based on particle swarm optimization wavelet support vector machine. *Rock Soil. Mech.* **2019**, *40*, 3662–3669.
26. Ling, T.; Qin, J.; Song, Q.; Hua, F. Intelligent displacement back-analysis based on improved particle swarm optimization and neural network and its application. *J. Railw. Sci. Eng.* **2020**, *17*, 2181–2190.
27. Chen, L.; Meng, J.D.; Li, Z.Z.; Xu, X.J.; Hao, L.; Ren, Y.X.; Zhao, Y. An optimized observation system and inversion method for fault detection based on surface-wave while tunneling. *J. Appl. Geophys.* **2024**, *228*, 105472. [[CrossRef](#)]
28. Wang, F.; Li, X.; Miao, L.; Xu, P. Mechanical parameters identification of surrounding rock based on wavelet SVM. *J. Hydroelectr. Eng.* **2010**, *29*, 184–190.
29. Kovacevic, M.S.; Bacic, M.; Gavin, K.; Stipanovic, I. Assessment of long-term deformation of a tunnel in soft rock by utilizing particle swarm optimized neural network. *Tunn. Undergr. Sp. Tech.* **2021**, *110*, 103838. [[CrossRef](#)]
30. Ma, J.J.; Li, T.B.; Yang, G.; Dai, K.K.; Ma, C.C.; Tang, H.; Wang, G.W.; Wang, J.F.; Xiao, B.; Meng, L.B. A real-time intelligent classification model using machine learning for tunnel surrounding rock and its application. *Georisk* **2023**, *17*, 148–168. [[CrossRef](#)]
31. Wei, W.; Jia, Y.; Sheng, Y.; Xu, G.; Yang, Y.; Zhang, D. Research on landslide susceptibility evaluation model based on I, SVM and I-SVM. *Saf. Environ. Eng.* **2023**, *30*, 136–144.
32. Zhang, Y.; Su, G.S.; Li, Y.; Wei, M.D.; Liu, B.C. Displacement back-analysis of rock mass parameters for underground caverns using a novel intelligent optimization method. *Int. J. Geomech.* **2020**, *20*, 04020035. [[CrossRef](#)]
33. Yan, H.H.; Liu, K.Y.; Xu, C.; Zheng, W.B. A novel method for identifying geomechanical parameters of rock masses based on a PSO and improved GPR hybrid algorithm. *Sci. Rep.* **2022**, *12*, 5670. [[CrossRef](#)]
34. Shen, Y.; Guo, B.; Gu, T. Particle swarm optimization algorithm and comparison with genetic algorithm. *J. Univ. Electron. Sci. Technol. China* **2005**, *34*, 696–699.
35. Kennedy, J.; Eberhart, R.C. Particle swarm optimization. In Proceedings of the IEEE International Conference on Neural Networks (ICNN 95), Perth, Australia, 27 November–1 December 1995.
36. Tang, J.; Liu, G.; Pan, Q.T. A review on representative swarm intelligence algorithms for solving optimization problems: Applications and trends. *IEEE-CAA. J. Automatic.* **2021**, *8*, 1627–1643. [[CrossRef](#)]
37. Jiang, A.N.; Wang, S.Y.; Tang, S.L. Feedback analysis of tunnel construction using a hybrid arithmetic based on Support Vector Machine and Particle Swarm Optimisation. *Autom. Constr.* **2011**, *20*, 482–489. [[CrossRef](#)]
38. Cortes, C.; Vapnik, V. Support-vector networks. *Mach. Learn.* **1995**, *20*, 273–297. [[CrossRef](#)]

39. Zhou, S.T.; Zhang, Z.X.; Luo, X.D.; Huang, Y.F.; Yu, Z.; Yang, X.W. Predicting dynamic compressive strength of frozen-thawed rocks by characteristic impedance and data-driven methods. *J. Rock Mech. Geotech.* **2024**, *16*, 2591–2606. [[CrossRef](#)]
40. Huang, Y.F.; Lei, Y.; Luo, X.D.; Fu, C. Prediction of compressive strength of rice husk ash concrete: A comparison of different metaheuristic algorithms for optimizing support vector regression. *Case Stud. Constr. Mat.* **2023**, *18*, e02201. [[CrossRef](#)]
41. Huang, Y.F.; Zhou, Z.K.; Li, M.Y.; Luo, X.D. Prediction of ground vibration induced by rock blasting based on optimized support vector regression models. *Cmes-Comp. Model. Eng.* **2024**, *139*, 3147–3165. [[CrossRef](#)]
42. Ran, Z.; Wu, J.X. Common energy decay indices of Saint-Venant's principle. *J. Eng. Mech.* **2008**, *25*, 14.

Disclaimer/Publisher's Note: The statements, opinions and data contained in all publications are solely those of the individual author(s) and contributor(s) and not of MDPI and/or the editor(s). MDPI and/or the editor(s) disclaim responsibility for any injury to people or property resulting from any ideas, methods, instructions or products referred to in the content.